PCCP

PAPER

View Article Online
View Journal | View Issue

Cite this: *Phys. Chem. Chem. Phys.*, 2016, **18**, 6239

Spectral assignments in the infrared absorption region and anomalous thermal hysteresis in the interband electronic transition of vanadium dioxide films

Peng Zhang,[a] Mengjiao Li,[a] Qinglin Deng,[a] Jinzhong Zhang,[a] Jiada Wu,[b] Zhigao Hu*[a] and Junhao Chu[a]

Received 2nd December 2015,
Accepted 28th January 2016

DOI: 10.1039/c5cp07416a

www.rsc.org/pccp

The metal–insulator transition (MIT) is of key importance for understanding the fundamental electronic interaction that determines the physical properties of vanadium dioxide (VO_2) film. Here, the spectral slopes of transmittance and reflectance in the infrared absorption region (about 0.62–1.63 eV) and the interband electronic transitions for VO_2 films with thicknesses of 27, 40 and 63 nm have been investigated. The potential applications of the spectral slopes were presented in detail. It is found that the variation of resistivity and transmittance increases with the spectral slopes of transmittance and reflectance. It is surprising that the resistivity of the VO_2 film with a thickness of 27 nm is larger than that of the VO_2 film with a thickness of 40 nm in the metal state. In addition, an anomalous counterclockwise thermal hysteresis with higher energy from the interband electronic transition was also found during the MIT process for the thinnest film. It is believed that this remarkable phenomenon could be related to the correlation effects in the rutile phase, which could lead to the splitting of the a_{1g} band into Hubbard bands. The lower Hubbard band would result in an electronic transition blue-shift with the empty e_g^{σ} band, which can explain the origin of the counterclockwise thermal hysteresis and the abnormal resistivity in the metal state.

1 Introduction

Vanadium dioxide (VO_2) is a paradigmatic example of a prototype correlated electron system that is vital for both fundamental physics and applications. It is generally known that the VO_2 shows an unusual first-order metal–insulator transition (MIT) around room temperature with a variation in electrical conductivity of several orders of magnitude.[1,2] Furthermore, a change of lattice structure from a high temperature, rutile ($P4_2/mn$) to a low temperature, monoclinic ($P2_1/c$) has been observed during the MIT process.[3,4] Several models have been proposed to account for the origin of the MIT process. The mechanism of the MIT can be electronically (Mott transition), structurally (Peierls transition) or collaboratively (Mott–Peierls transition) driven, and is usually associated with the electronic ordering phenomenon.[5–7] Because of the complicated relationship between the electron–lattice coupling and the electron–electron interactions, the origin of and the fundamental mechanism driving the transition are still controversial.

Due to its prominent optical and electrical properties, VO_2 is a promising candidate for a variety of applications, such as in sensor devices, modulators, and optical and electrical switching.[8–10,12] The MIT properties could be manipulated using not only temperature, but also electric fields, strain, doping and pressure *etc.*[13–16] In the past several decades, the impact of the above factors on the internal mechanism of MIT has been studied widely. A lot of interesting and new phenomena were found through various kinds of measurement techniques. However, the effect of the thickness on the energy transition was often ignored and scarcely investigated. It is well known that the dynamics of the electronic correlations may substantially differ from the conventional physics when the film thickness is relatively thin. The interband transitions can be affected by altering the film thickness, which has important implications in a correlated system with Coulomb repulsion between electrons and orbital overlaps. Therefore, it is necessary to provide additional insight into the underlying mechanism of the energy transition for the cases of films with different thicknesses.

In this study, the VO_2 films with different thicknesses were prepared using pulsed laser deposition (PLD). The spectral slopes of transmittance and reflectance in the infrared absorption region

[a] *Key Laboratory of Polar Materials and Devices, Ministry of Education, Department of Electronic Engineering, East China Normal University, Shanghai 200241, China. E-mail: zghu@ee.ecnu.edu.cn; Fax: +86-21-54345119; Tel: +86-21-54345150*

[b] *Department of Optical Science and Engineering, Fudan University, Shanghai 200433, China*

were elucidated in detail. It is found that the resistivity in the metal state does not decrease with the film thickness, which can be ascribed to the variation of the carrier concentration. In addition, an anomalous counterclockwise thermal hysteresis behavior in a higher energy transition was found for the thinnest VO_2 film. It is believed that the remarkable phenomenon could be related to the correlation effects in the rutile phase, which is the origin of the abnormal resistivity and counterclockwise thermal hysteresis behavior.

2 Experimental details

2.1 Fabrication, microstructure, optical and electrical characterization of VO_2 films

The films were synthesized using a pulsed laser deposition (PLD) technique and the systematic study of the growth conditions can be found elsewhere.[17] Atomic force microscopy (AFM: Digital Instruments Icon, Bruker) was used to characterize the surface morphology of the VO_2 films. To evaluate the thickness and observe the surface microstructure of the VO_2 films, scanning electron microscopy (SEM: Philips XL30FEG) was performed. X-ray diffraction (XRD) with Cu Kα radiation (λ = 0.1542 nm) was used to characterize the crystal structure of the films. To analyze the electrical properties, the resistance as a function of the temperature with different thicknesses was measured using a THMSE 600 heating/cooling stage (Linkam Scientific Instruments) in a temperature range from 273 to 373 K. In order to determine the components and valence states, X-ray photoelectron spectroscopy (XPS, AXIS Ultra^{DLD}, Japan) with Al Kα radiation ($h\nu$ = 1486.6 eV) was carried out at room temperature under vacuum. The temperature-dependent transmittance spectra and near-normal incident (about 8°) reflectance spectra were recorded using a double beam ultraviolet-infrared spectrophotometer (PerkinElmer Lambda 950) at a photon energy from 0.46 to 6.52 eV (190–2650 nm).

3 Results and discussion

3.1 Microstructure analysis

Atomic force microscopy (AFM) images of the films are shown in Fig. 1(a)–(c). It can be seen that the VO_2 films include many individual grains and the size of the nanoparticles increases with the film thickness. Fig. 1(d)–(f) show the high resolution scanning electron microscopy (SEM) pictures of the VO_2 films, which reveal that the samples consist of homogeneous and continuous nanoparticles. It can be found that the size of the grains also increases gradually with the film thickness, which is consistent with the AFM results. From the cross section shapes in Fig. 1(g)–(i), the film thickness is about 27, 40 and 63 nm. Fig. 2(a) shows the XRD diffraction patterns in a regular θ–2θ scanning mode for the VO_2 films with different thicknesses. The peaks located at 2θ = 27.92° correspond to the (011) plane for the VO_2 films. It is found that the position of the (011) peak is nearly the same for each film thickness, which demonstrates that the strain is almost relaxed between the interface of the film and substrate. This can also be reflected by the T_{MIT} extracted from the differential hysteresis loops of the resistivity and transmittance. The full width at half maximum of the (011) peaks decreases with the film thickness, which illustrates that the crystal quality can be improved with the film thickness.

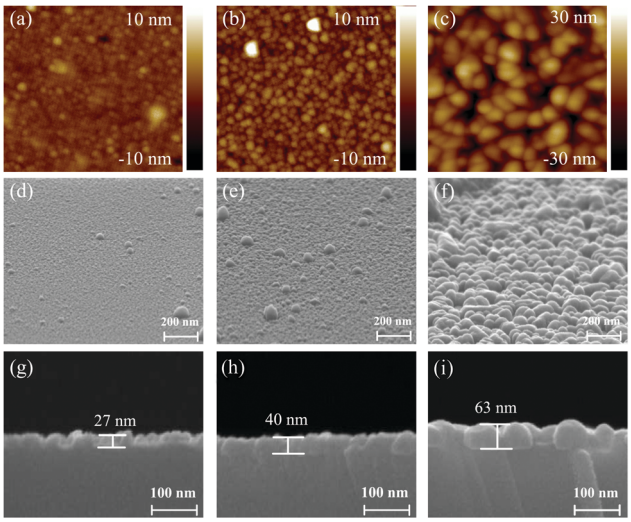

Fig. 1 (a–c) AFM images of the VO_2 films with thicknesses of 27, 40 and 63 nm. (d–f) The high resolution SEM pictures of the VO_2 films with different thicknesses. (g–i) The cross section shapes of the films.

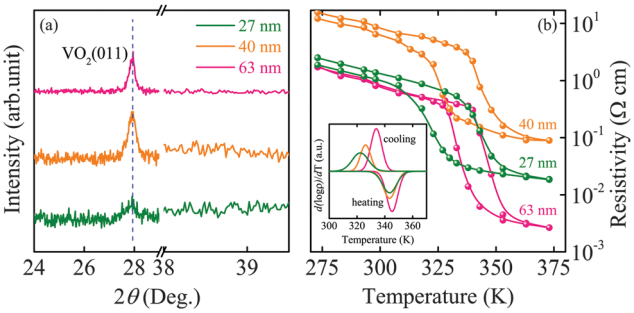

Fig. 2 (a) The θ–2θ scan XRD curves for thickness dependent VO_2 films. (b) The resistivity as a function of temperature for the VO_2 films with different thicknesses. The inset shows differential curves of the resistivity.

3.2 Electrical transport

The resistivity change during a heating–cooling cycle across the transition regime is shown in Fig. 2(b). The inset presents the differential curves of the resistivity hysteresis loops. In order to analyze and compare the transport behavior of the VO_2 films, the parameters of the electrical properties have been extracted from the related differential curves fitted using a Gaussian function, wherein T_c represents the phase transition temperature. The discrepancy of the T_c between the heating and cooling process was defined as ΔT_c. The phase transition magnitude and the resistivity at the metal state was denoted as ΔA and R_ρ, respectively. The parameters are presented in Table 1. It can be seen that the variation of the resistivity for the VO_2 films with thicknesses of 27, 40 and 63 nm is 133, 175 and 875, which increases with the film thickness. It is worth noting that the

Table 1 The parameters of the electrical and optical properties extracted from the related differential curves fitted using a Gaussian function

Samp. (nm)	T_c (K)	F (K)	ΔT_c (K)	ΔA	ΔTr	R_ρ	R_{Tr}
27	343.4	5.08	21.1	133	0.32	0.0187	0.49
40	343.4	4.46	17.3	175	0.44	0.0892	0.36
63	345.2	3.94	11.4	875	0.54	0.0026	0.18

resistivity drop for the VO_2 films with thicknesses of 27 and 40 nm is more than a magnitude of 10^2 and about 10^3 for the thickest film. The results are in good agreement with other reports for VO_2 films with different thicknesses.[13,18,19] Generally, the resistivity decreases in the metal state with the film thickness. However, it is surprising that the resistivity in the metal state seems to disobey this rule for the VO_2 films with the thicknesses of 27 and 40 nm. It is believed that the cracked or twinned structure can lead to the higher resistivity and the phase transition magnitude of the resistivity and transmittance can be reduced.[20,21] Nevertheless, the phase transition magnitude of the resistivity and transmittance increases with the film thickness, which indicates that the effect of the crack or the twinned structure can be ignored in the present work. It is generally agreed upon that the degree of the metallization is closely related to the carrier concentration. Thus, the abnormal resistivity in the metal state can be accounted for by a large change in carrier density.

3.3 XPS survey spectra

In order to analyze the components and valence states, X-ray photoelectron spectroscopy (XPS) was carried out at room temperature under vacuum. The chemical element of C1s with a binding energy of 285 eV was used to calibrate the spectra. The overall core level XPS survey spectrum of the VO_2 film with a thickness of 40 nm is shown in Fig. 3(a). The V 2p and O 1s spectra of the films with different thicknesses are presented in Fig. 3(b)–(g). The Lorentzian–Gaussian sum function was used for dividing the V 2p and O 1s peaks, and can be used to evaluate the chemical state and stoichiometry of the film.[22,23] From the V $2p_{2/3}$ peaks, it can be found that there are two peaks located at about 515.5 and 516.9 eV, which can be assigned to the oxidation states of V^{4+} and V^{5+}, respectively.[10,11,25,26] The observation of V^{5+} peaks is not surprising as the XPS is a surface characterization technique. In addition, the variation of the annealing conditions also affects the formation of the valence states and the VO_2 film surface is prone to oxidation after being exposed to the atmosphere. The main peak located at about 530 eV can be assigned to O 1s and the additional components with O 1s, located at about 531.5 eV, can be assigned to the C–O and C=O bonds, which may come from the surface adsorption oxygen or the sample preparation process.[22] To estimate the concentrations of atoms and the stoichiometry in a homogeneous system, the following general relation was used:[24]

$$N_{V^{4+}} = \frac{A_{V^{4+}}F_{V^{5+}}}{A_{V^{4+}}F_{V^{5+}} + A_{V^{5+}}F_{V^{4+}}}. \quad (1)$$

$$N_{V^{5+}} = \frac{A_{V^{5+}}F_{V^{4+}}}{A_{V^{4+}}F_{V^{5+}} + A_{V^{5+}}F_{V^{4+}}}. \quad (2)$$

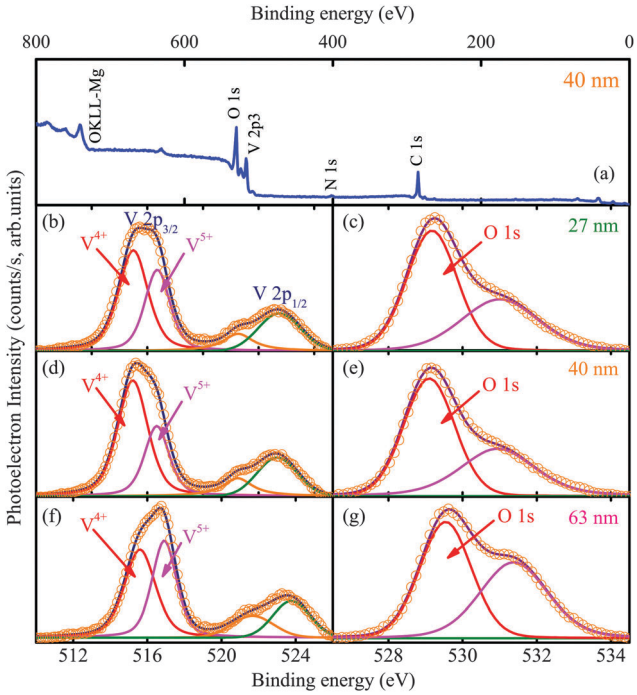

Fig. 3 (a) Overall core level XPS spectrum for the VO_2 film with a thickness of 40 nm. (b–g) XPS spectra of V 2p lines and O 1s lines with the Lorentzian–Gaussian dividing peak analysis for the VO_2 films with thicknesses of 27, 40 and 63 nm.

$$R_{O/V} = \frac{A_{O1s}F_{O1s}}{A_{V2p_{3/2}}F_{V2p_{3/2}}}. \quad (3)$$

Where A is the peak intensity of the atom, and F is the sensitivity factor. N and R are the atomic concentration and the V : O ratio. Note that the $F_{V^{4+}}$ and $F_{V^{5+}}$ have been taken as the same (F = 1). $F_{V2p_{3/2}}$ and F_{O1s} is 1.3 and 0.66, respectively. Through the calculation using the equations, the stoichiometry is $VO_{1.965}$, $VO_{1.943}$ and $VO_{1.955}$ for the VO_2 films with thicknesses of 27, 40 and 63 nm, respectively. The V^{4+} and V^{5+} valences were evaluated and found to have fraction percentages of 61.8% and 38.2%, 63% and 37%, 60.3% and 39.7%, respectively. It is found that the stoichiometry and the percentages of V^{4+} and V^{5+} agree with each other for the three films, which indicates that the compositional homogeneity is almost the same.

3.4 Optical properties and electronic structures

3.4.1 NIR-UV transmittance spectra. Fig. 4(a)–(c) show the temperature-dependent transmittance changes of the VO_2 films with different thicknesses. The variation of the transmittance (ΔTr) at selected incident photon energies ($h\nu$ = 0.468 eV, λ = 2650 nm) during the heating process is 0.32, 0.44 and 0.54. The variation of the transmittance increases gradually with the film thickness, which is in good agreement with the resistivity variation in Fig. 2(b). In order to visualize the transmittance change, the hysteresis loops of transmittance at a wavelength of 2650 nm are shown in Fig. 4(e). The differential curves of the transmittance hysteresis loops are shown in Fig. 4(h), from which the T_{MIT} is about 338 K, 339 K and 341 K and the full width at half

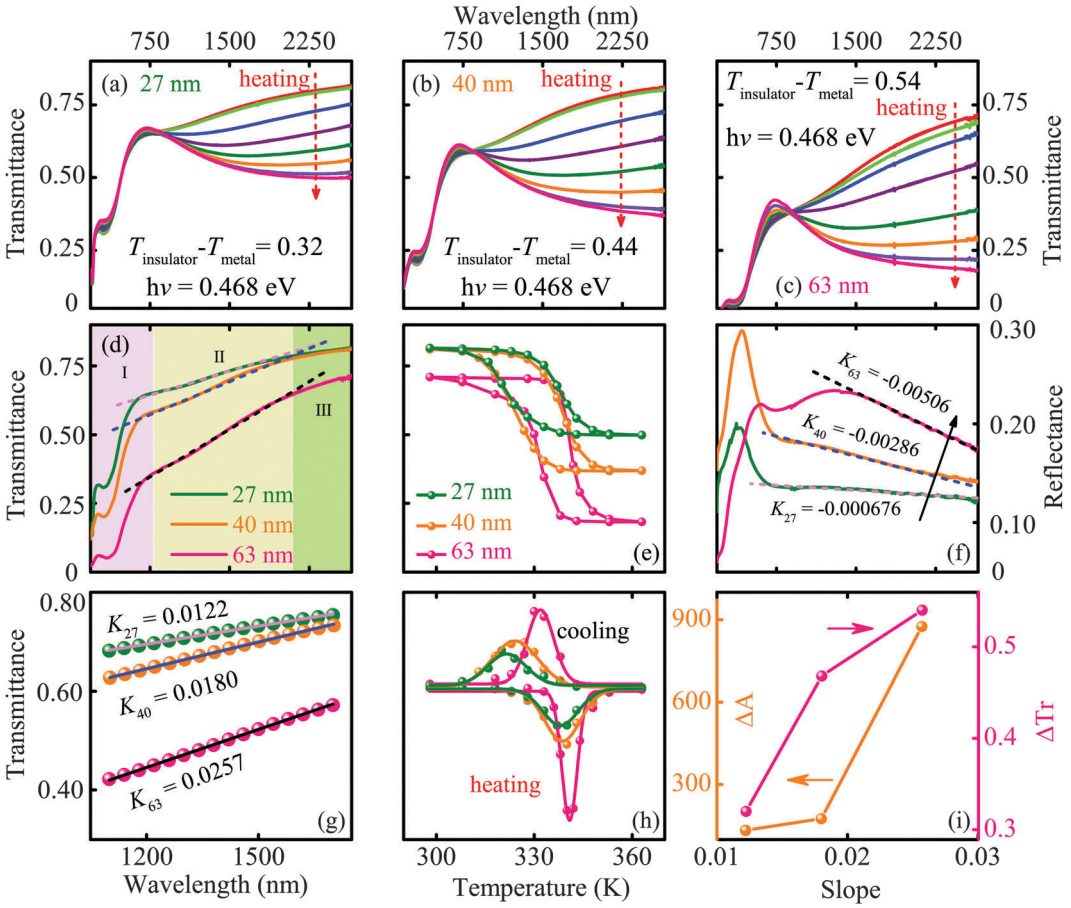

Fig. 4 (a–c) The transmittance spectra for the VO_2 films with different thicknesses. (d) The room temperature transmittance for the films with different thicknesses. (e) and (h) show the hysteresis loops for the temperature dependence of transmittance at a wavelength of 2650 nm and the differential curves, respectively. (f) The reflectance spectra for the VO_2 films with different thicknesses. (g) The fitting curves of the transmittance in the infrared region. (i) The relationship between the spectral slope and the variation of transmittance and resistivity.

maximum decreases with the film thickness. It should be noted that the transmittance in the metal state (R_{Tr}) is 0.49, 0.36 and 0.18 for the VO_2 films with thicknesses of 27, 40 and 63 nm, which indicates that the degree of metallization increases with the film thickness. However, it was found that the degree of metallization reflected by the transmittance at the metal state is not consistent with that for the electrical behavior. For comparing the variation trend of the resistivity and transmittance at the metal state, the relevant parameters are listed in Table 1.

3.4.2 NIR-UV reflectance spectra and spectral slope at infrared absorption region. The room temperature transmittances shown in Fig. 4(d) are collected together to compare the slopes of the spectra. The transmittance spectra were divided into three ranges, the ultraviolet-visible (190–760 nm, 6.52–1.63 eV) region (defined by I), the near-infrared absorption (760–2000 nm, 1.63–0.62 eV) region (defined by II) and the infrared (2000–2650 nm, 0.62–0.46 eV) region (defined by III). It can be seen that the main difference in the spectra in Section III is the variation of the transmittance. The shape and variation trends of the spectra have little discrepancy. In Section 1, the change of the transmittance is inconspicuous. In Section II, the divergence of the transmittance and variation trends of the spectra is obvious, especially the conditions for the thickest VO_2 film (63 nm). It can be found that the slope of the spectra in Section II increases with the film thickness. The transmittance spectra in region II are equivalent to a straight line. The fitting results are shown in Fig. 4(g). The slope of the spectra is 0.0122, 0.0180 and 0.0257 for the VO_2 films with thicknesses of 27, 40 and 63 nm, respectively. Based on the XRD data, transport behavior and the transmittance hysteresis loops, it can be concluded that the spectral slopes in the near-infrared absorption region have positive correlations with the phase transition magnitude of the resistivity and transmittance for the VO_2 films with different thicknesses. In addition, a similar phenomenon can also be observed using the room temperature reflectance for the three films, which is shown in Fig. 4(f). Furthermore, from the transmittance done by Li *et al.*,[27] the spectral slope also has a positive correlation with the variation of the transmittance for the films with different thicknesses.

Fig. 4(i) presents the relationship between the spectral slope and ΔA and ΔTr. It can be found that ΔA and ΔTr increase with the slope, which indicates that the spectral slope has a positive correlation with the variation of the transmittance and resistivity for the VO_2 films with different thicknesses. Therefore, it can be concluded that the variation trend of the electrical and optical

properties can be judged conveniently from the spectral slope. It is well known that the band gap of VO_2 films is about 0.6 eV and the transition energy from the lower V 3d filled a_{1g} band to the empty e_g^{π} band belongs to the energy range of about 0.62–1.82 eV in the insulator state.[28–31] In the metal state, the a_{1g} band overlaps the e_g^{π} and the band gap is reduced to zero. That is to say, the variation of the electronic structure is mainly reflected by the change in the two bands. It is worth noting that the energy range of region II is 1.63–0.62 eV, which is larger than the band gap while belonging to the energy range of the transition between the two bands. Therefore, the degree of the phase transition can be reflected using the divergence of the transmittance in region II in the insulator state.

3.4.3 Theoretical calculation of the transmittance. It was found that the degree of metallization reflected by the electrical behavior in the metal state is not consistent with that of the transmittance. In order to investigate the abnormal phenomenon, the transmittance was fitted to obtain the energy transition, A_D and B_D, which is closely related to the carrier concentration. The Drude–Lorentz (DL) oscillator dispersion relation is used to simulate the transmittance spectra, as the following

$$\varepsilon(E) = \varepsilon_\infty - \frac{A_D}{E^2 + iEB_D} + \sum_{k=1}^{3} \frac{A_k}{E_k^2 - E^2 - iEB_k}. \quad (4)$$

where ε_∞ is the high-frequency dielectric constant. A_k, E_k, B_k and E is the amplitude, center energy, broadening of the jth oscillator and the incident photon energy, respectively. The parameter A_D is the square of the plasma frequency and B_D is the electron collision or damping frequency. The fitting parameters are listed in Table 2.

It was mentioned above that the parameter A_D is the square of the plasma frequency, which is closely related to the carrier concentration n ($A_D = ne^2/\varepsilon_0\varepsilon_\infty m^*$). Where the ε_0 is the permittivity of free space, m^* is the conductivity effective mass. It can be taken that the A_D is proportional to the carrier concentration on the condition of unity electron average effective mass.[31–33] It is worth noting that the B_D is nearly the same for the three VO_2 films, which indicates that the carrier mobility ($\mu = e/2\pi m^* cB_D$) is almost identical in the metal state. The value of A_D is 7.18, 6.87 and 7.85 and B_D is 0.10, 0.12 and 0.13 for the three films, respectively. Based on the values of A_D and B_D, it can be concluded that the overall variation of the carrier concentration increases with the film thickness. However, the value of A_D for the 27 nm film is larger than that of the 40 nm film, which indicates that the carrier concentration for the 27 nm film is larger than that of the 40 nm film. Therefore, the abnormal resistivity in the metal state can be ascribed to the variation of the carrier concentration. This also demonstrates that the internal mechanism reflected by the electrical and optical results in the metal state is consistent.

3.4.4 The dielectric function and comparison of the n_{eff}. In order to increase the reliability and make a contrast, we probed the phenomenon through the n_{eff}. The *f*-sum rule and spectral weight was used to calculate the parameter n_{eff}, the equation can be written as the following:[31,34]

$$n_{eff}(\omega_c) = \frac{2m_0 V}{\pi e^2} \int_0^{\omega_c} \sigma_r(\omega) d\omega. \quad (5)$$

Wherein $\sigma_r = \varepsilon_0 \omega \varepsilon_i$ and the equation can be defined in the following form:

$$n_{eff}(\omega_c) = \frac{2\varepsilon_0 m_0 \omega V}{\pi e^2} \int_0^{\omega_c} \varepsilon_i(\omega) d\omega. \quad (6)$$

Where, σ_r and ε_i is the real part of the optical conductivity and the imaginary part of the dielectric constant as a function of photon energy $\hbar\omega$, respectively. The imaginary part of the dielectric constant is shown in Fig. 5. It is believed that 95% of the spectral weight can be recovered using 4 eV, which indicates that the *f*-sum rule is still not fully satisfied at such high energies.[34] That is to say, the *f*-sum rule is appropriate for the range with lower energies. It is interesting to find that the dielectric function is sequential between the energy range of (0.47–2.37 eV) while it is chaotic beyond 2.37 eV. The energy range of 0.47–2.37 eV is within the transition energy of the filled lower a_{1g} band to the empty e_g^{π} band or the empty upper a_{1g} band during the MIT process. We believe that the regular result is not a coincidence and rather a manifestation of the overlapping of the a_{1g} band with the e_g^{π} band. A similar phenomenon can also be observed from the spectral slope at the near-infrared absorption region. If the n_{eff} increases with the film thickness, the dielectric function will be presented at a regularity in a certain energy range.

Table 2 Parameters of the Drude–Lorentz (DL) model for the VO_2 films extracted from the best fitting transmittance spectra at several temperatures. The 90% confidence limits are given in parentheses

Samp.	27 nm		40 nm		63 nm	
T (K)	298	363	298	363	298	363
A_1	1.54 (0.01)	5.82 (0.22)	1.37 (0.01)	4.96 (0.15)	1.26 (0.03)	6.22 (0.12)
B_1 (eV)	1.55 (0.02)	0.93 (0.01)	1.30 (0.01)	0.90 (0.01)	0.972 (0.02)	0.91 (0.01)
E_1 (eV)	1.23 (0.01)	0.67 (0.02)	1.25 (0.01)	0.65 (0.01)	1.22 (0.01)	0.67 (0.01)
A_2	3.32 (0.01)	2.57 (0.04)	2.97 (0.05)	2.38 (0.06)	5.28 (0.04)	3.36 (0.06)
B_2 (eV)	2.17 (0.02)	1.81 (0.06)	1.91 (0.04)	1.52 (0.04)	2.09 (0.02)	1.39 (0.03)
E_2 (eV)	3.61 (0.01)	3.34 (0.01)	3.37 (0.01)	3.14 (0.01)	3.14 (0.01)	2.90 (0.01)
A_3	2.38 (0.041)	2.61 (0.13)	1.42 (0.04)	1.42 (0.02)	2.33 (0.06)	1.68 (0.03)
B_3 (eV)	1.74 (0.07)	3.35 (0.27)	4.82 (0.50)	4.43 (0.37)	4.82 (0.38)	3.93 (0.30)
E_3 (eV)	6.06 (0.02)	6.41 (0.13)	6.33 (0.12)	5.74 (0.07)	6.45 (0.13)	5.30 (0.05)
A_D	—	7.18 (0.19)	—	6.87 (0.05)	—	7.85 (0.41)
B_D (eV)	—	0.10 (0.02)	—	0.12 (0.01)	—	0.13 (0.03)

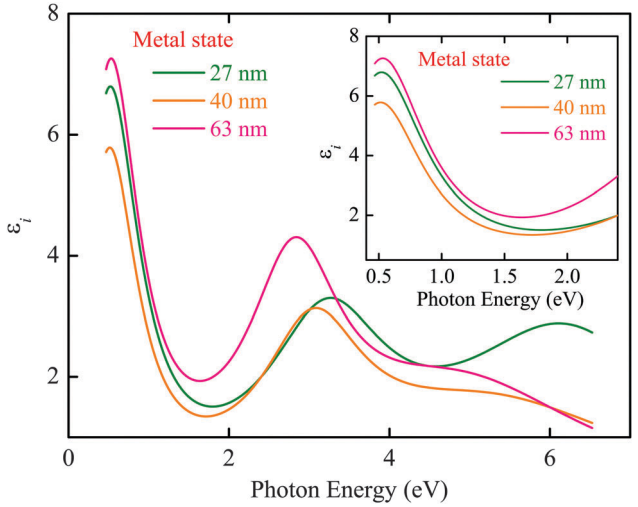

Fig. 5 The dielectric function of the VO_2 film with different thickness at metal state. The inset shows the dielectric function at infrared wavelength range.

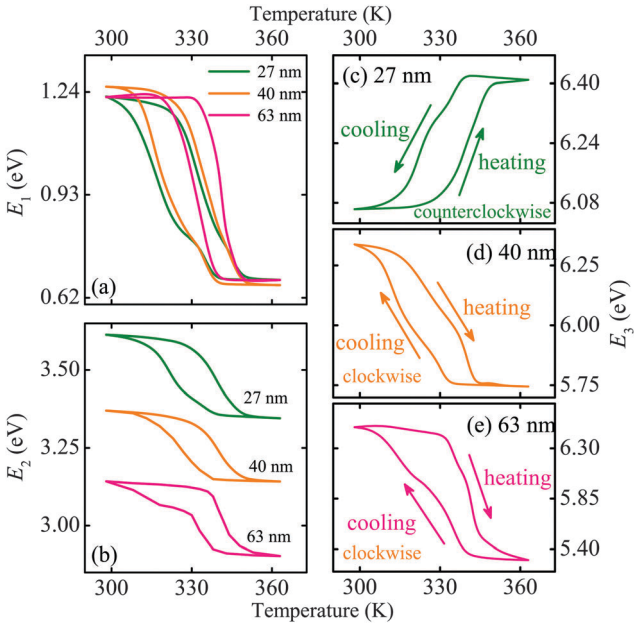

Fig. 6 (a) and (b) The electronic transition of E_1 and E_2 for the VO_2 films with different thicknesses, respectively. (c–e) The hysteresis loop of the electronic transition of E_3 for the VO_2 films.

Therefore, the dielectric function was divided into two segments, with energy ranges of 0.47–2.37 eV and 2.37–6.53 eV.

Because the *f*-sum rule is not satisfied at higher energy and the n_{eff} is closely related to the variation of the a_{1g} and e_g^{π} bands, the dielectric function with the energy range at 0.47–2.37 eV was used to compare the n_{eff} for the three films. The inset presents the dielectric function in the infrared range. We assume that $f_1(\omega_c)$, $f_2(\omega_c)$ and $f_3(\omega_c)$ represent the dielectric function at a certain energy for the VO_2 films with thicknesses of 27, 40 and 63 nm, respectively. Obviously, the relationship of the dielectric function is $f_3(\omega_c) > f_1(\omega_c) > f_2(\omega_c)$ at the energy range of 0.47–2.37 eV. Based on eqn (6), the relationship of the n_{eff} is $n_{\text{eff3}} > n_{\text{eff1}} > n_{\text{eff2}}$ at the certain energy range, where the volume V can be taken as 1/2 in the metal state.[33] Through the internal mechanism obtained using transmittance spectra, it can be concluded that the peculiar resistivity in the metal state can be attributed to the variation of the carrier concentration. Generally, the carrier concentration will be increased with the film thickness. Thus, it is confusing that the carrier concentration of the film with a thickness of 27 nm is larger than that for the film with a thickness of 40 nm. It was believed that the occurrence of the Hubbard band may be a sign of the increased overlapping of the a_{1g} band to the e_g^{π} band.[34]

3.5 Electronic transition and band structure

From the fitting results, three center energies can be assigned to the following electronic transitions:[36] (1) lower V3d filled a_{1g} band to the empty e_g^{π} band (E_1); (2) the filled O2p band to the empty e_g^{π} band (E_2); (3) lower V3d filled a_{1g} to the empty e_g^{σ} band (E_3). In this study, E_1 and E_2 represent the conventional thermal hysteresis as a function of temperature, which is shown in Fig. 6(a) and (b). However, an abnormal hysteresis was found for the thinnest film with a thickness of 27 nm. The hysteresis loop of the electronic transition of E_3 is shown in Fig. 6(c)–(e). Surprisingly, it can be found that E_3 exhibits a counterclockwise hysteresis loop for the thinnest film while E_3 shows a clockwise hysteresis loop for the other two films. A similar phenomenon was previously found in the magnetization and resistivity of $La_{1-x}Sr_xMnO_3$.[35] They believed that the abnormal thermal hysteresis can be attributed to the competing interaction of different metal phases. According to the conventional band theory, the lower and upper Hubbard bands (LHB and UHB, respectively) were not considered. Correlation effects in the rutile phase could lead to a degree of splitting of the a_{1g} into lower and upper Hubbard bands.[37] It was believed that the Hubbard bands played a key role in the prominence of the pseudogap-type transition from the filled a_{1g} band to the empty e_g^{π} band.[34] In addition, the lower Hubbard band has been seen previously in photoemission experiments on bulk VO_2.[38]

E_3 is the transition of filled a_{1g} to the empty e_g^{σ} band in the insulator and metal states. It is well known that the a_{1g} band will be shifted up during the MIT process and overlap with the e_g^{π} band, which indicates that the energy of E_3 decreases with the temperature. However, the E_3 variation is contrary to the conventional perspective. Taking the Hubbard band into consideration, the counterclockwise hysteresis loop can be ascribed to the Hubbard bands splitting from the a_{1g} band. The schematic energy levels in the insulator and metal states for the VO_2 film with a thickness of 27 nm are shown in Fig. 7(a) and (b). Assuming the splitting of the a_{1g} band continuously during the MIT process, the lower Hubbard band will shift down and keep steady state in the metal state. This will lead to the transition energy of E_3 being blue-shifted during the MIT process. Therefore, the counterclockwise hysteresis behavior can be observed. Taking into account the thickness of the film, we believe the correlation effects are more easily influenced by the interfacial effect for the thinnest film. Furthermore, the

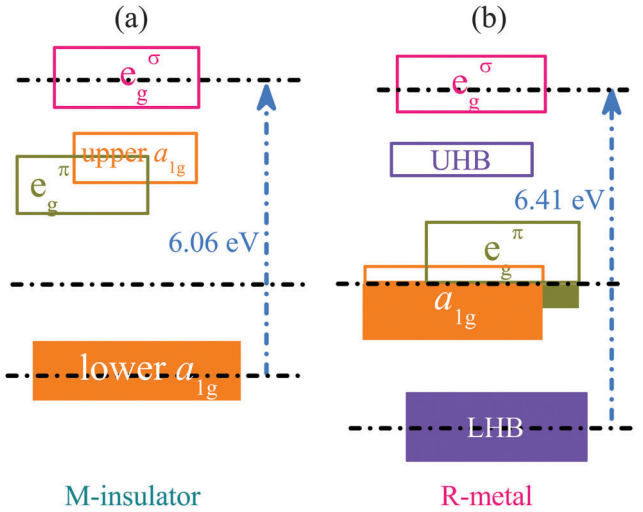

Fig. 7 (a) and (b) Schematic energy levels in the insulator and metal states for the VO_2 film with a thickness of 27 nm, respectively.

occurrence of the Hubbard bands may symbolize the increased overlapping of the a_{1g} band to the e_g^{π} band, which may be the origin of the abnormal resistivity at the metal state. Therefore, the counterclockwise hysteresis loop of E_3 can be observed for the VO_2 film with a thickness of 27 nm.

4 Conclusions

In summary, it was found that the spectral slopes in the near-infrared absorption region have a positive correlation with the phase transition magnitudes of the resistivity and transmittance for VO_2 films with different thicknesses. This finding is of benefit for discerning and forecasting the optical and electrical properties of films from the macroscopic level. In addition, abnormal resistivity in the metal state was observed. The parameters of the Drude model and the *f*-sum rule were applied to account for the phenomenon, which can be attributed to the variation of the carrier concentration. Remarkably, the E_3 energy exhibits a counterclockwise hysteresis loop with temperature for the VO_2 film with a thickness of 27 nm, which can be ascribed to the occurrence of the Hubbard bands. It is believed that the lower Hubbard band may lead to the transition of E_3 being blue shifted and symbolize the increased overlapping of the a_{1g} band with the e_g^{π} band.

Acknowledgements

This work was financially supported by the Major State Basic Research Development Program of China (Grant No. 2013CB922300 and 2011CB922200), the Natural Science Foundation of China (Grant No. 11374097, 61376129 and 61504156), the Projects of Science and Technology Commission of Shanghai Municipality (Grant No. 15JC1401600, 14XD1401500, 13JC1402100, and 13JC1404200), and the Program for Professor of Special Appointment (Eastern Scholar) at Shanghai Institutions of Higher Learning.

References

1 F. J. Morin, *Phys. Rev. Lett.*, 1959, **3**, 34–36.
2 P. Baum, D. S. Yang and A. H. Zewail, *Science*, 2007, **318**, 788–792.
3 C. Kubler, H. Ehrke, R. Huber, R. Lopez, A. Halabica, R. F. Haglund and A. Leitenstorfer, *Phys. Rev. Lett.*, 2007, **99**, 116401.
4 D. Wegkamp, M. Herzog, L. Xian, M. Gatti, P. Cudazzo, C. L. McGahan, R. E. Marvel, R. F. Haglund Jr, A. Rubio, M. Wolf and J. Sthler, *Phys. Rev. Lett.*, 2014, **113**, 216401.
5 R. M. Wentzcovitch, W. W. Schulz and P. B. Allen, *Phys. Rev. Lett.*, 1994, **72**, 3389.
6 T. M. Rice, H. Launojs and J. P. Pouget, *Phys. Rev. Lett.*, 1994, **73**, 3042.
7 M. M. Qazilbash, M. Brehm, B. G. Chae, P. C. Ho, G. O. Andreev, B. J. Kim, S. J. Yun, A. V. Balatsky, M. B. Maple, F. Keilmann, H. T. Kim and D. N. Basov, *Science*, 2007, **318**, 1750–1753.
8 L. Pellegrino, N. Manca, T. Kanki, H. Tanaka, M. Biasotti, E. Bellingeri, A. S. Siri and D. Marre, *Adv. Mater.*, 2012, **24**, 2929–2934.
9 N. Shukla, A. V. Thathachary, A. Agrawal, H. Paik, A. Aziz, D. G. Schlom, S. K. Gupta, R. E. Herbert and S. Datta, *Nat. Commun.*, 2015, **6**, 7812.
10 Y. Zhou, J. Park, J. Shi, M. Chhowalla, H. Park, D. A. Weitz and S. Ramanathan, *Nano Lett.*, 2015, **15**, 1627–1634.
11 S. Chen, J. J. Liu, L. H. Wang, H. J. Luo and Y. F. Gao, *J. Phys. Chem. C*, 2014, **118**, 18938–18944.
12 A. Tselev, J. D. Budai, E. Strelcov, J. Z. Tischler, A. Kolmakov and S. V. Kalinin, *Nano Lett.*, 2011, **11**, 3065–3073.
13 B. A. Nagaphani, X. G. Alexander, D. Marc, C. Matteo, G. Li, H. R. Alexander, K. Roopali, O. Hendrik, A. J. Catherine, A. Elke, P. R. Kevin, A. U. Hermann, G. S. Mahesh and S. P. P. Stuart, *Nat. Phys.*, 2013, **9**, 661–666.
14 T. X. Nan, M. Liu, W. Ren, Z. G. Ye and N. X. Sun, *Sci. Rep.*, 2012, **4**, 5931.
15 C. Marini, E. Arcangeletti, D. D. Castro, L. Baldassare, A. Perucchi, S. Lupi, L. Malavasi, L. Boeri, E. Pomjakushina, K. Conder and P. Postorino, *Phys. Rev. B: Condens. Matter Mater. Phys.*, 2008, **77**, 235111.
16 L. G. Bai, Q. Li, S. A. Corr, Y. Meng, C. Y. Park, S. V. Sinogeikin, C. Ko, J. Q. Wu and G. Y. Shen, *Phys. Rev. B: Condens. Matter Mater. Phys.*, 2015, **91**, 104110.
17 P. Zhang, K. Jiang, Q. L. Deng, Q. H You, J. Z. Zhang, J. D. Wu, Z. G. Hu and J. H. Chu, *J. Mater. Chem. C*, 2015, **3**, 5033–5040.
18 D. Brassard, S. Fourmaux, M. J. Jacques, J. C. Kieffer and M. A. El Khakani, *Appl. Phys. Lett.*, 2005, **87**, 051910.
19 R. Molaei, R. Bayati, F. Wu and J. Narayan, *J. Appl. Phys.*, 2014, **115**, 164311.
20 K. Nagashima, T. Yanagida, H. Tanaka and T. Kawai, *Phys. Rev. B: Condens. Matter Mater. Phys.*, 2006, **74**, 172106.
21 X. Li, A. Gloter, H. Gu, X. Cao, P. Jin and C. Colliex, *Acta Mater.*, 2013, **61**, 6443–6452.
22 S. Rathi, I. Lee, J. H. Park, B. J. Kim, H. T. Kim and G. H. Kim, *ACS Appl. Mater. Interfaces*, 2014, **6**, 19718–19725.
23 Z. Yang and S. Ramanathan, *Appl. Phys. Lett.*, 2011, **98**, 192113.

24 Q. W. Shi, W. X. Huang, Y. X. Zhang, J. Z. Yan, Y. B. Zhang, M. Mao, Y. Zhang and M. J. Tu, *ACS Appl. Mater. Interfaces*, 2011, **3**, 3523–3527.
25 N. F. Quackenbush, J. W. Tashman, J. A. Mundy, S. Sallis, H. Paik, R. Misra, J. A. Moyer, J. H. Guo, D. A. Fischer, J. C. Woicik, D. A. Muller, D. G. Schlom and L. F. J. Piper, *Nano Lett.*, 2013, **13**, 4857–4861.
26 C. H. Chen and Z. Y. Fan, *Appl. Phys. Lett.*, 2009, **95**, 262106.
27 M. Li, X. Wu, L. Li, Y. X. Wang, D. B. Li, J. Pan, S. J. Li, L. T. Sun and G. H. Li, *J. Mater. Chem. A*, 2014, **2**, 4520–4523.
28 W. T. Liu, J. Cao, W. Fan, Z. Hao, M. C. Martin, Y. R. Shen, J. Wu and F. Wang, *Nano Lett.*, 2011, **11**, 466–470.
29 W. W. Li, Q. Yu, J. R. Liang, K. Jiang, Z. G. Hu, J. Liu, H. D. Chen and J. H. Chu, *Appl. Phys. Lett.*, 2011, **99**, 241903.
30 A. Gavinit and C. C. Y. Kwan, *Phys. Rev. B: Solid State*, 1972, **5**, 3138.
31 H. W. Verleur, A. S. Barker and C. N. Berglund, *Phys. Rev.*, 1968, **172**, 788–798.
32 K. Okazaki, H. Wadati, A. Fujimori, M. Onoda, Y. Muraoka and Z. Hiroi, *Phys. Rev. B: Condens. Matter Mater. Phys.*, 2004, **69**, 165104.
33 D. B. Mcwhan, M. Marezio, J. P. Remeika and P. D. Dernier, *Phys. Rev. B: Solid State*, 1974, **10**, 490.
34 T. J. Huffman, P. Xu, A. J. Hollingshad, M. M. Qazilbash, L. Wang, R. A. Lukaszew, S. Kittiwatanakul, J. Lu and S. A. Wolf, *Phys. Rev. B: Condens. Matter Mater. Phys.*, 2015, **91**, 205140.
35 J. Dho, W. S. Kim and N. H. Hur, *Phys. Rev. Lett.*, 2001, **87**, 187201.
36 W. W. Li, J. J. Zhu, X. F. Xu, K. Jiang, Z. G. Hu, M. Zhu and J. H. Chu, *J. Appl. Phys.*, 2011, **110**, 013504.
37 S. Biermann, A. Georges, A. Lichtenstein and T. Giamarchi, *Phys. Rev. Lett.*, 2001, **87**, 276405.
38 T. C. Koethe, Z. Hu, M. W. Haverkort, C. S. Langeheine, F. Venturini, N. B. Brookes, O. Tjernberg, W. Reichelt, H. H. Hsieh, H. J. Lin, C. T. Chen and L. H. Tjeng, *Phys. Rev. Lett.*, 2006, **97**, 116402.

